Proceedings of the ASME 2010 3rd Joint US-European Fluids Engineering Summer Meeting and 8th International Conference on Nanochannels, Microchannels, and Minichannels
FEDSM-ICNMM2010
August 1-5, 2010, Montreal, Canada

FEDSM-ICNMM2010-30571

Refractive Index Matching with Distortion Measurements in a Bed of Irregularly Packed Spheres

Vishal A. Patil
Mechanical Engineering
Oregon State University
Corvallis, Oregon 97331

James A. Liburdy
Mechanical Engineering
Oregon State University
Corvallis, Oregon, 97331

ABSTRACT
Experimental flow visualization in porous media is often conducted using optical techniques such as PIV and PTV for velocity field estimation and LIF for concentration field measurements. The porous bed is made optically accessible to laser light and imaging by matching refractive indices of the liquid phase to that of the solid matrix, including the channel walls. The methods most commonly employed to match the refractive indices have been to maximize the transmitted intensity through the bed or to rely on refractometers for measurement of the liquid and solid phases. Refractometers with sensitivity of 0.001 could still cause refraction problems in a porous bed, while accuracy and sensitivity of transmission based methods are limited by the camera resolution and noise scattered by impurities and stray light caused by reflections at interfaces. Both these methods fail to provide uncertainty estimates for particle position determination due to slight refractive index mismatching. This work presents a method for assessing the matching of refractive indices that relies on measuring distortion of a target when imaged through a porous bed. The target used is a grid of 250 μm dots irradiated with light at the necessary wavelength at which refractive indices are to be matched. Two principle types of distortion are quantified, distortion of the image centroid due to interface refraction and intensity distortion within the image for index mismatching as low as 0.0005.

INTRODUCTION
Flow in porous media is frequently encountered in many engineering and natural processes such as gas adsorption, filtration, combustion, catalytic reactors, groundwater hydrology and others. The physical aspects of flows in porous media have been discussed in many books such as Bear [1], Scheidegger [2] and others.

The investigation of the flow characteristics in porous media has proven to be elusive due to the difficulty of interrogation access, the range of flow passage scales typically found, and the inherent three dimensional nature of the flow, among other difficulties. Optical methods like PIV [3, 4, 5], PTV [6, 7, 8, 9, 10], LIF [11, 12, 13, 14] and LDA [15, 16] have been in use to study the transport properties in various types of porous media. In order to achieve proper optical access and to minimize distortion, refractive index matching (RIM) has been employed to essentially make the bed transmissive to the optical probe or light sheet. Other methods have also been used such as positron emission tomography [17] and magnetic resonance imaging [18, 19, 20] and generally represent a very large investment in the imaging technique, but can provide high quality three-dimensional information.

In addition to allowing for proper probe access, the design of the porous media test facility is also challenging. For instance, packing of the media imposes certain flow conditions that affect the global flow characteristics like overall pressure drop and dispersion [21, 22]. Also, the test bed dimensions relative to the

characteristic pore size is important in understanding wall effects. Empirical studies show that a minimum of five bead diameters away from the wall is needed to effectively reduce wall effects in studies using spherical beads to form the porous media [23]. Although this may not seem to be overly constraining, this minimum distance requirements implies that the optical access needs to be able to probe through a significant number of fluid/solid interfaces in the imaging process. Consequently a slight mismatch in the refractive indices between the solid and liquid phases may result in significant loss of spatial resolution and signal intensity caused by refraction and reflection.

The choice of seed particles is typically very important in either PIV or PTV. The goals include the need to accurately following the flow features while providing an optimal image size to minimize errors such as peak locking, and to achieve accurate displacement peak estimates [24]. The use of different wavelengths of light to probe the test section versus that used to image data imposes inherent mismatch of index of refraction due to wavelength dependence on index of refraction. Examples where this issue is of importance include the use of fluorescent microspheres which use the detection of emission light from a rather narrow bandwidth [4, 9] while laser induced fluorescence, LIF, looks at broadband fluorescent light to determine dye concentration [11, 12, 14]. Other broadband detection methods have employed scattering of broadband illumination for particle detection [7, 8, 10]. Since refractive index matching must be performed at a particular wavelength of light, errors will occur. In general, liquids tend to show a greater change in index with changing wavelength than do solids. This implies that if RIM is obtained at a particular wavelength, variations in wavelength in the experiment due to a different light source wavenumber or because of changes in the use of fluorescence will result in mismatches, with potential error in the determination of particle position. Liquids typically used to perform RIM can be grouped into three classes, aqueous organic, aqueous inorganic and non-polar organic. Typically the liquids can be tuned to properly match the solid phase and walls of the test bed at a given index of refraction determined by the solid phase [25, 26].

To achieve proper focus most imaging systems allow focal adjustment in order to increase the intensity and obtain better edge distinction. Proper care must be taken to obtain the focal adjustment using the wavelength of imaged light, which again may be different than that used to obtain RIM [10, 11, 12]. Consequently image distortion will occur and single sources will appear as multiple images [27].

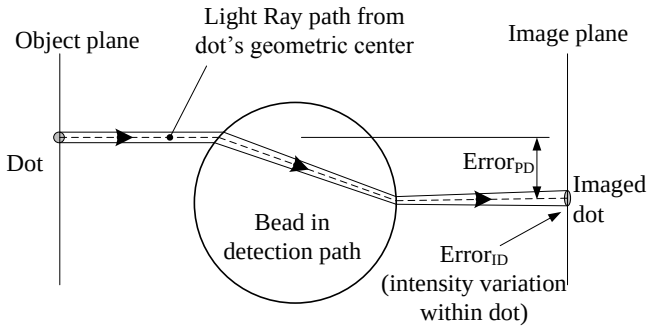

Figure 1: Schematic depicting sources of errors in imaging a dot.

This study focuses on the use of index of refraction matching, such as used in PIV and PTV, to resolve flow in porous media. In particular, the degree to which refractive index mismatch occurs between the liquid phase and solid phase is of concern in the ability to accurately locate tracer particle center of mass positions. There are several methods available to determine the refractive index, n_D, directly using a refractometer, or index matching by maximizing the measured transmission of light through the porous bed, both are discussed here.

Two types of errors are identified in this study. First, the geometric center of the dot, its centroid, will be distorted due to refraction at each solid-liquid interface, as shown in Fig. 1. The error introduced in the detected position due to this effect is identified as Error$_{PD}$. Second, the intensity within the dot will be distorted due to local variations in surface radius of curvature experienced by light rays emerging from the dot. This error is also affected by surface roughness, an example of which is also shown in Fig. 1. This second effect will lead to increased errors of identify the image center when using methods like center of mass and Gaussian curve fitting which use the local intensity distribution to estimate dot centers. This error is identified as Error$_{ID}$.

To quantify errors in this study a measure of distortion is estimated using a fixed grid of points imaged through the porous media. The centroid method [28] is used to track the image distortion and displacement of individual points. Uncertainties are presented in the determination of particle position versus increasing wavelength bandwidth for three liquids representing the classes of liquids identified above, glycerol (aqueous organic), sodium iodide (aqueous inorganic) and silicone oil (non-polar organic). The index of refraction relationships given in [26] are used. The goal is to present

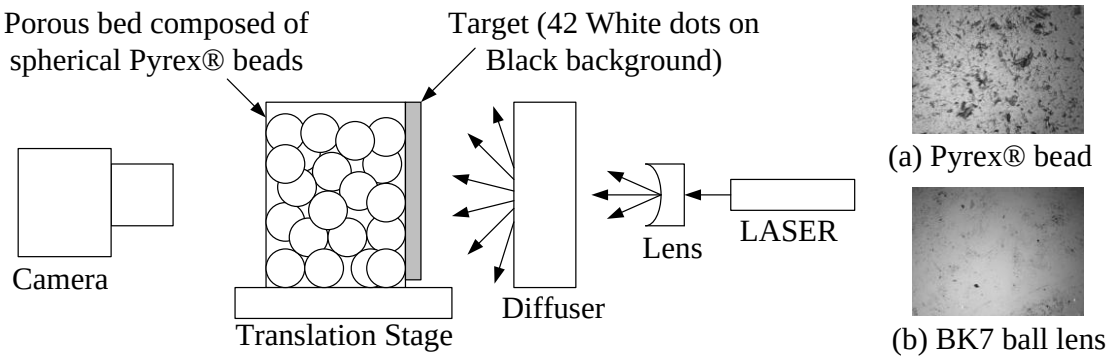

Figure 2: Schematic of the experimental test set-up used to record images. Surface images of (a) Pyrex bead used in current setup compared to surface of a (b) BK7 ball lens

results that will aid in the proper design of RIM for optical access in porous media and to assess the level of uncertainties involved with RIM.

EXPERIMENTAL SET-UP

Figure 2 shows the experimental apparatus used for this study. The work was performed for a porous bed of size 40 mm x 40 mm x 60 mm and bead size of 6 mm (Pyrex®). Ammonium thiocyanate (NH_4SCN) was the liquid phase used to match the refractive index by varying the concentration. The liquid refractive index, n_D, was measured using a refractometer (Atago co., Model: R5000), with resolution of 0.001 evaluated at the sodium D line, 589.3 nm. The target used for imaging consisted of an array of 250 μm diameter dots arranged in a 6x7 array but with the center dot being 1 mm diameter as shown in Figure 2. The target was backlight illuminated with a Nd-YLF laser system (New Wave Research, Model: Pegasus PIV). The laser light wavelength used was 527 nm. The imaging system included a CMOS camera (Integrated Design Tools Inc., Model: MotionPro™ X-3) fitted with an adjustable focusing lens (Nikon Model: AF Micro-NIKKOR 60mm f/2.8D). Imaging was accomplished using lens settings of f/2.8 and a focal distance for the case when the liquid and solid phases were matched of 0.24 m. The camera magnification for this setup was measured such that the images was 18.25 μm/pixel.

In setting up the experiment the bed was first filled with fluid phase only. The target was placed behind the cell as shown in Fig. 2. The lens focus was adjusted to give a sharp image with diffuse white light illumination. Then an image of the bed with only liquid phase was taken with laser light illumination. This image was used as the control image for estimating errors due to position distortion and intensity distortion arising from inclusion of the solid phase. Beads were then added to the bed and a second image of the target was captured. The laser light intensity was increased and a third image of the target was acquired. At this point the lens focus was readjusted to give the sharpest image possible and then a fourth image was taken. The series of images taken for the case of n_D equal to 1.470 is shown in Fig. 3. Note that the intensity scale of the images is inverted for visible presentation. The control image for each value of n_D from 1.466 to 1.474 was the image taken through the test section with only the liquid phase.

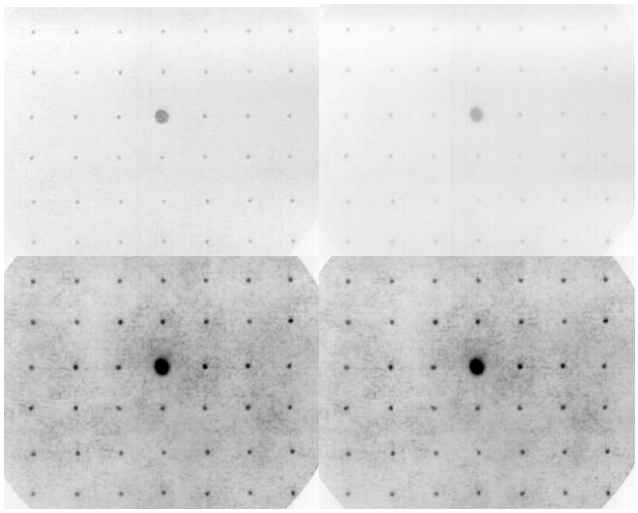

Figure 3: Images taken for n_D = 1.470; (a) imaging through the test section with liquid phase only, (b) imaging with both liquid and solid phases, (c) as in (b) but at a higher light intensity, (d) as in (c) but readjusted focus.

DATA ANALYSIS

The transmittance of the bed was determined from images of the larger central dot of the array shown in Fig. 3 for each n_D. The same central dot was also used to estimate errors associated with fitting a curve to the intensity distribution for purposes of particle center estimation. This was done utilizing images shown in Figure 3(a) and

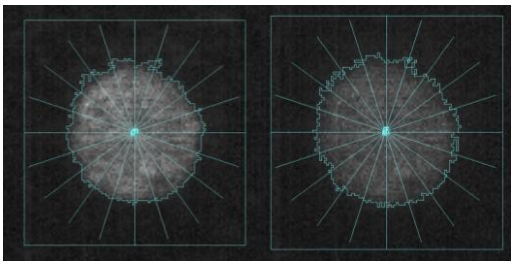

Figure 4: Illustration of the methodology for the central 1 mm dot detection applied to the $n_D = 1.469$ case. In 100 x 100 pixel^2 interrogation window, the threshold was adjusted to find only one particle, where, a particle is a contiguous pixel above the threshold. The centroid method is used to estimate the dot center. Ten equally angularly spaced lines are drawn through the centroid to estimate intensity distortion within the dot. Here (a) is the magnified view showing the dot boundary selection for the central 1mm dot imaged through the porous bed with the liquid phase only, the control image (b) is the dot boundary selection for the center spot imaged through the bed with both liquid and solid phases present.

3(b) for n_D=1.470. The method outlined by Feng et al. [28] was used to identify the dots and find their centers. The method was implemented in IMAGEJ software. The general method is as follows. The lowest threshold of the image was determined to find the dot centroid. Then a 100 x 100 pixel^2 interrogation window about each dot center was used. The lowest local threshold for the interrogation window was found to detect the dot boundary. Results are illustrated in Fig. 4(a) and 4(b).

The transmittance, T, was determined from the spatially integrated intensity for the center dot as

$$T = \frac{I - I_{Dark}}{I_{CTL} - I_{Dark}} \qquad (1)$$

where I, I_{CTL} and I_{Dark} are the spatially integrated intensity of the image, the integrated intensity of the control image of the central dot, and a dark image (no illumination), respectively.

The estimate of the distortion of the location of the center due to intensity variations with and without beads was determined by using ten equally angularly spaced and equal length lines passing through the centroid as shown in Fig. 4. Each line was used to determine distance of its center of mass from dot centroid based on the intensity distribution along the line, $l_{m,i}$. The particle position error due to intensity distortion within a dot was then evaluated using all ten lines from:

$$Error_{ID} = \sqrt{\frac{1}{10}\sum_{i=1}^{10}\left[l_{m,i} - l_{m,i,CTL}\right]^2} \qquad (2)$$

where $l_{m,i,CTL}$ is the distance between center of mass and centroid of each line determined from the control (no bead) image and the summation is over the ten individual lines.

An additional distortion based on the relative position of all of the dots in the image array was also determined. To do this the images in Figure 3(a) and 3(c) were analyzed for a range of values of n_D. First the dot centers were determined for the control image using a local threshold in each of the 100 x 100 pixel^2 interrogation windows about each dot. The errors in the X and Y coordinate of the centers were estimated using errors associated with the relative displacement differences for all adjacent dots in the array referenced to the dot separation in the control image. The resulting expressions for errors of x and y displacements become:

$$Error_{PD,x} = \sqrt{\frac{1}{N_m\left(N_n - 1\right)}\sum_{r=1}^{N_m}\sum_{c=1}^{N_n - 1}\left(\left(X_{m,n+1} - X_{m,n}\right) - \left(X_{m,n+1} - X_{m,n}\right)_{CTL}\right)^2}$$

$$Error_{PD,y} = \sqrt{\frac{1}{N_n\left(N_m - 1\right)}\sum_{n=1}^{N_n}\sum_{m=1}^{N_m - 1}\left(\left(Y_{m+1,n} - Y_{m,n}\right) - \left(Y_{m+1,n} - Y_{m,n}\right)_{CTL}\right)^2} \qquad (3)$$

the total error is given by:

$$Error_{PD} = \sqrt{\left(Error_{PD,x}\right)^2 + \left(Error_{PD,y}\right)^2} \qquad (4)$$

The same method was used to estimate the particle position error after the focus was adjusted with beads in the bed, based on images associated with those shown in Fig. 3(c) and 3(d) for each values of n_D.

The determination of the appropriate index match of liquid-solid phases was based on the measured errors as:

$$n_{D,match} = \frac{\sum Error_{PD} n_D}{\sum Error_{PD}} \qquad (5)$$

Here $Error_{PD}$ was evaluated using Eqn. (4) and n_D of the liquid was measured using the refractometer at the sodium D line wavelength. It should be noted that the case of n_D = 1.474 was not included in the Eqn. (5) because it was considered an outlier due to the presence of multiple images, which is discussed later.

The refractive index mismatch between the liquid and solid phases, $(n_L - n_S)$, was determined based on the Cauchy dispersion equation, see [26]:

$$n_1 - n_2 = C_L\left(\frac{1}{\lambda_1^2} - \frac{1}{\lambda_2^2}\right) \quad (6)$$

where C_L is a constant and a property of the liquid and λ_i is the wavelength at which n_i is evaluated. If n_1 is set to some arbitrary value of index of refraction at λ, say n_L, and n_2 is the index when matching occurs with the solid phase, that is n_S, the relationship between index of refraction difference versus wavelength variation can be determined. In addition, using eqn. (6) it is possible to express (n_L-n_S) at any wavelength to the difference between n_D and $n_{D,match}$ as:

$$(n_L - n_S) = (n_D - n_{D,match}) \quad (7)$$

where the right hand side is at a reference wavelength, such as sodium D line. In arriving at this expression the variation of n_S is assumed small, which is typical of solids compared with liquids. Consequently the measured value of the right hand side can be used to determine the liquid-solid mismatch at any other wavelength.

The error in particle center determination due to position distortion associated with using fluorescent emission of bandwidth $\Delta\lambda$ for particle detection can also be determined using Eqn. (6). If the fluorescence emission occurs over a finite bandwidth, then distortion will occur even if the index matching occurs at the peak emision wavelength. The amount of distortion will depend on the wavelength dependent emission spectrum, $f(\lambda)$, as well as the transmittance through the bed, $T(\lambda)$. So here n_1 is set to the index associated with an arbitrary wavelength within the emission bandwidth and n_2 equal to the index at the maximum emission, which is equal to n_S for matching. Based on this the following discrete integration is used over the wavelength

$$Error_{PD,\Delta\lambda} = \frac{\sum_{\lambda=\lambda_{em}}^{\lambda_{em}+\Delta\lambda} fTError_{PD}}{\sum_{\lambda=\lambda_{em}}^{\lambda+\Delta\lambda} fT} \quad (8)$$

where both f and T are then transformed into functions of (n_L-n_S) using Eqn. (6). The experimental data for the bed transmittance are used to find $Error_{PD,\Delta\lambda}$; specifically the data shown in Fig. 9 was used based on a linear curve fit through the data. Also, the function f needs to be specified for a given specific fluorescent dye. Lastly,

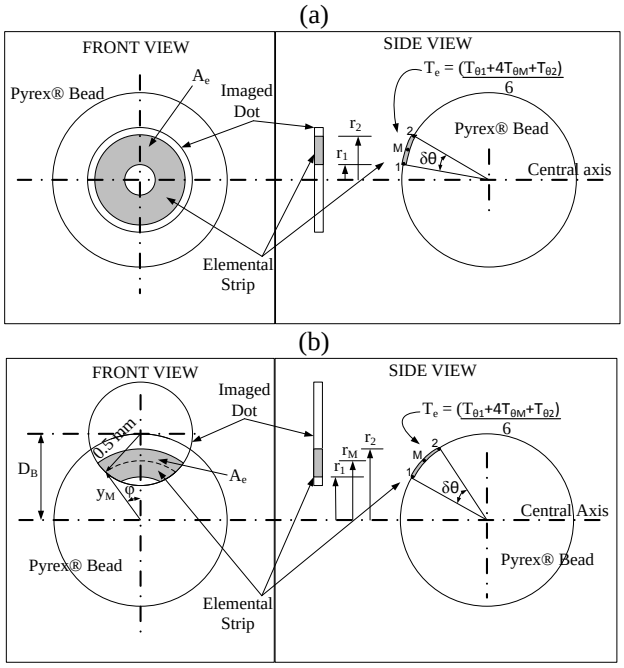

Figure 5: Illustration of the geometry used in the numerical model to estimate transmittance through a bead; for the case where (a) the dot center matches the bead center, and (b) the dot center matches the bead edge.

$Error_{PD}$ is evaluated using a curve fit for particle position error versus $|n_L - n_S|$, shown in Fig. 7.

Numerical Model for Estimating Transmission

The transmission of light through the bed will result in distortion of the intensity distribution. In order to estimate the effect of an individual bead on the transmission, a model was constructed using ray tracing accounting for the location of the dot center to be recorded relative to the bead location. Figure 5(a) illustrates the geometry used where the imaged dot is aligned with a bead center along the optical axis. Figure 5(b) shows the case of the dot center aligned with the edge of the bead.

The center dot surface was segmented into 1000 elements, where one element is shown in gray in Fig. 5. For each element, the transmittance was estimated using Fresnel's equation [29]:

$$T_\theta = \frac{1}{2}\left(\frac{n_t\cos\theta_t}{n_i\cos\theta}\right)\left[\left(\frac{2n_i\cos\theta}{n_i\cos\theta + n_t\cos\theta_t}\right)^2 + \left(\frac{2n_i\cos\theta}{n_i\cos\theta_t + n_t\cos\theta}\right)^2\right], \quad \text{for } \theta < \theta_c \quad (9)$$

$$T_\theta = 0, \text{ for } \theta \geq \theta_c \quad (10)$$

where subscripts i and t are for incident and transmitted light, respectively, θ_t is the angle of refraction for the transmitted ray and was found using Snell's law of refraction, and θ_c is the critical angle of reflection.

Simpson's rule was applied to find the total transmittance for each element. The transmittance at each interface for a single bead was obtained by summing over all 1000 elements, accounting for both light entering and leaving the bead. The total porous bed transmittance was determined by assuming the total number of beads intersected by a light ray to be the length of the bed divided by the bead diameter, L/D_B equivalent to taking the bead transmittance to the power L/D_B.

Since a random packing of the bed is assumed the transmittance can vary from light ray to light ray since different angles of incidence occur at different positions on the bead-liquid interface. Two cases were evaluated to determine the extent of transmission variations, (i) an imaged dot aligned with the center of the bead, Fig. 5(a) and (ii) an imaged dot aligned its center with an edge of the bead, Fig. 5(b). For either of these cases the transmittance at the interface can be taken as:

$$T_{L-S} = \frac{\sum T_e A_e}{\sum A_e} \qquad (11)$$

where A_e is the surface area intersected by the bead of the image light from the dot for each element, as shown in Fig. 5 by the shaded areas for the two cases of alignment.

RESULTS

The goal of this study is to quantify the distortion of even small mismatches in index of refraction between the solid and liquid phases. Results are organized to illustrate the errors in identifying the centroid of imaged light sources, such as from seed particles within the flow. Also errors are evaluated based on those associated with distortion of images that would result in errors of applying a curve fitting to the imaged source due to intensity distortion. Errors are also presented in terms of a mismatching of the index of refraction based on differences of wavelength for the imaging process such as may occur when using a fluorescent dye emission for seed detection while using the excitation wavelength for index matching. Finally, the situation of multiple image occurrence is discussed relative to the excitation wavelength.

First, the impact of refractive index mismatch on the focal length is determined. The focal length was estimated from the scale on the camera lens for images in Fig. 3(c) and 3 (d) and is shown to have a systematic increase for those cases with n_D of 1.468, 1.467, and 1.466 (this corresponds to differences o liquid index less than the solid of -0.0014, -0.0024, -0.0034, respectively). Alternatively, the focusing length shows a decrease for cases with a liquid index of 1.471, 1.472, 1.473 and 1.474

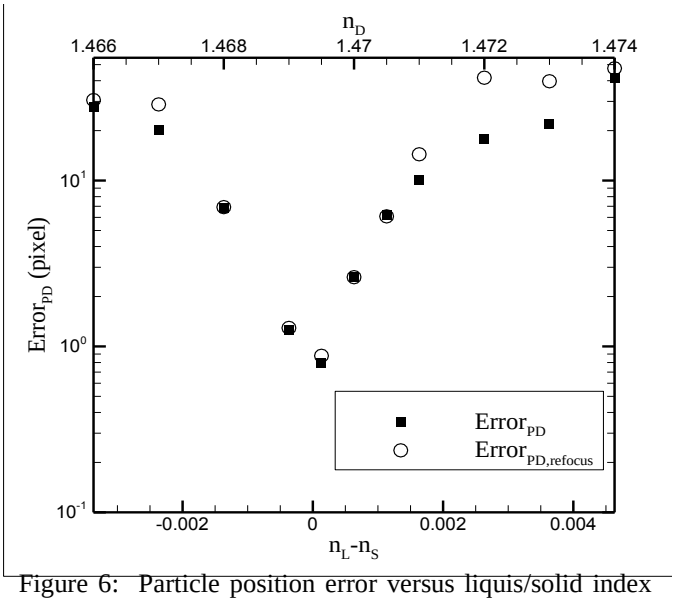

Figure 6: Particle position error versus liquis/solid index mismatch, n_L-n_S using Equation (4).

(a positive refractive index mismatch of 0.0016, 0.0026, 0.0036 and 0.0046, respectively). For index of refraction differences less than 0.0011 there was no discernable change in the focusing distance.

The reason for the shift in the focal length can be explained by the fact that the Pyrex® beads act as lenses. The focal length of a lens is inversely proportional to $(n_S - n_L)$ and proportional to the diameter of the bead. Consequently, when the refractive index mismatch $(n_L - n_S)$ is negative/positive, the beads act as a converging/diverging lens and the resultant focal distance increases/decreases. In a randomly packed bed of arbitrary size the focal distance shifts that occur will vary with bead size, number of bead intersections of the light path and total path length.

The errors associated with the determination of the centroid position of the imaged dots using Eqn. (5) are given in Fig. 6 using data before and after refocusing to obtain the sharpest image. There is some differences introduced by readjusting the focus once the mismatch is greater than 0.002. It should be noted that multiple images are seen for mismatches that exceeds 0.002, and is discussed later. Subsequent results are presented for data obtained without refocusing.

To better show trends of $Error_{PD}$, the results are replotted in Fig. 7 using a log-log plot. The resultant linear trend can be explained from the following argument based on ray bending of each bead. The lens power, P_s is given as a function of index of refraction mismatch, see [29], as:

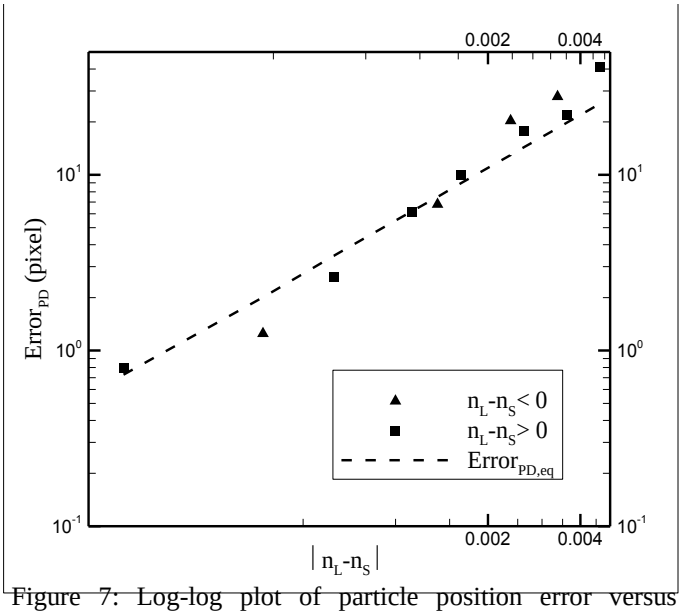

Figure 7: Log-log plot of particle position error versus liquis/solid index mismatch, n_L-n_S, using Equation (4).

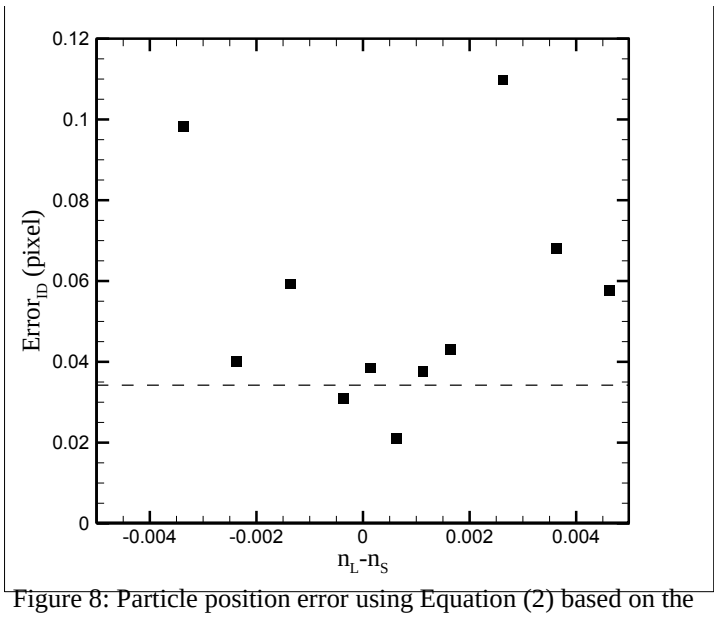

Figure 8: Particle position error using Equation (2) based on the centroid identification from intensity distributions. The dashed line represents the resolution of the method. It comes from error associated with drawing a line through centroid can be as high as 0.5 pixel.

$$P_S = \frac{4}{D_B}\left(\frac{n_S - n_L}{n_L}\right) \tag{12}$$

where D_B indicates the bead diameter. If this is extended to a multiple bead bed with L/D_B representing the effective number of beds across the optical path of the bed, then the bed power can be expressed as

$$P_{BED} = \frac{L}{D_B} P_S \tag{13}$$

If the magnification, M, is specified for a given imaging system as

$$M = \frac{N_B D_B}{1000} \tag{14}$$

where N_B is the number of beads imaged per 1000 pixels (an arbitrary number here), then the error expressed in number of pixels is inversely proportional to M estimated as:

$$Error_{PD} \propto \frac{L}{N_B D_B^3}\left(\frac{n_S - n_L}{n_L}\right) \tag{15}$$

Since in the experiments carried out here L, N and D_B are all constant and the magnitude of the mismatch is much smaller than the index of refraction, or n_L is approximately constant, the observed linear relationship with the index mismatching is apparent.

The particle position error (in pixels) due soley to intensity distortion versus index mismatch $(n_L - n_S)$ is shown in Fig. 8 based on Eqn. (2). The scale for $Error_{ID}$ has been normalized to an image that is 3 pixels in diameter (that is, errors for the imaged central dot which are 62 pixels in diameter are scaled by the factor 3/62. The dashed horizontal line in the figure represents the resolution limit of this analysis method. There is no apparent systematic trend other than as index mismatching increases the likelihood of increased error does occur. This random nature is most likely a result of the surface roughness. It should be noted that the magnitude of this error affects particle centroid identification but here is much smaller than the position error shown in Fig. 6.

The effect of index mismatch on the total transmittance is shown in Fig. 9. The expected peak occurs near perfect matching of indices, at least to within a mismatch of 0.0015. The decrease of transmittance is nearly symmetric and decreases by approximately one-half as the mismatch reached approximately 0.0035.

The data of Figure 9 are replotted in Figure 10 on a log-log scale using the absolute value of the mismatched index of refraction. The transmittance decays essentially linearly with mismatch over the range studied. To help interpret this trend the transmittance was calculated for the light path of a circular image passing through L/D_B beads where the spot center lines up with the bead centers, shown as line C-C in Fig. 10. Also included are the results for when the spot center lines up with the edge for the beads denoted as line C-E. Clearly the drop in transmittance is dominated by the low transmittance of light intensity near the edges of the beads. That is to say light passing through the bead center will have little loss

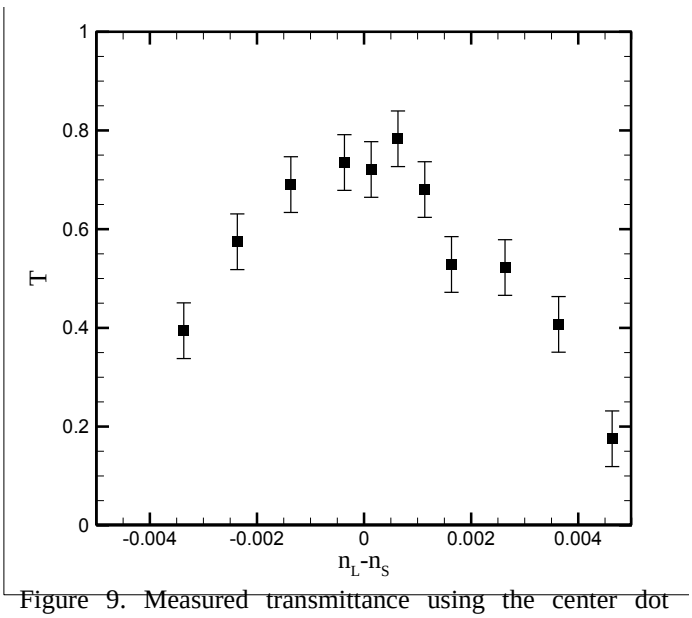

Figure 9. Measured transmittance using the center dot versus liquis/solid index mismatch, n_L-n_S

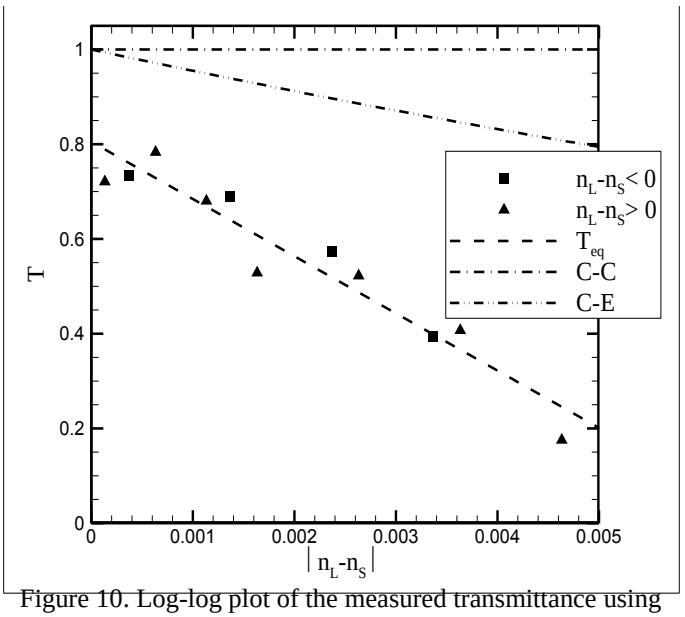

Figure 10. Log-log plot of the measured transmittance using the center dot versus liquis/solid index mismatch, n_L-n_S

of transmittance and the loss increases as the rays pass further and further from the bead center because of the increasing incidence angle. This model does not take into account the random packing of beads in the bed which could only be assessed statistically for a randomly packed bed. The slope of the transmittance decay would be expected to approach that of the experimental results for a more random packing as more light rays pass through interfaces near the edges of beads.

Another effect of index of refraction mismatching is the wavelength variation between the light source and the wavelength of the collected light being imaged due to index variation with wavelength. Further, spatial distortion will occur when using a very wide bandwidth of the light source or emission in the case of fluorescent imaging. To illustrate this effect the following example is used. Three different liquid phases are used: acrylic matching oil [Cargille-Sacher Laboratories Inc, Code 5032], glycerol [30], sodium iodide solution [26] while the solid phase is assumed to have no relative change in refractive index versus wavelength. A seed particle is taken as orange fluorescent (540/560) FluoSpheres® polystyrene microspheres (Molecular Probes, Inc.)

The results using Eqn. (8) are shown in Fig. 11, where the fluorescence emission, *f*, was evaluated only using the bandwidth emission for wavelengths greater than the peak since the emission curve typically drops rapidly on the shorter wavelength side. Results show that when the bandwidth is greater than approximately 5 nm, the expected error is above 1 pixel. This analysis can be used to estimate the bandwidth of emitted and detected light to keep this error at an acceptable level.

The occurrence of multiple images from a single image source can occur as the index mismatch increases. In the experiments conducted here when the mismatch in refractive index was greater than 0.002 multiple images were observed. They have been observed before for the simple case of imaging particles through curved walls [27]. Control experiment for multiple images is shown in Fig. 12 where reference images were obtained using a sodium lamp (589.3 nm wavelength), with the liquid index n_D of 1.474 and images were also taken with a laser light source (527 nm wavelength) using the laser light source results in multiple images for both focused and defocused images. For other cases the defocused

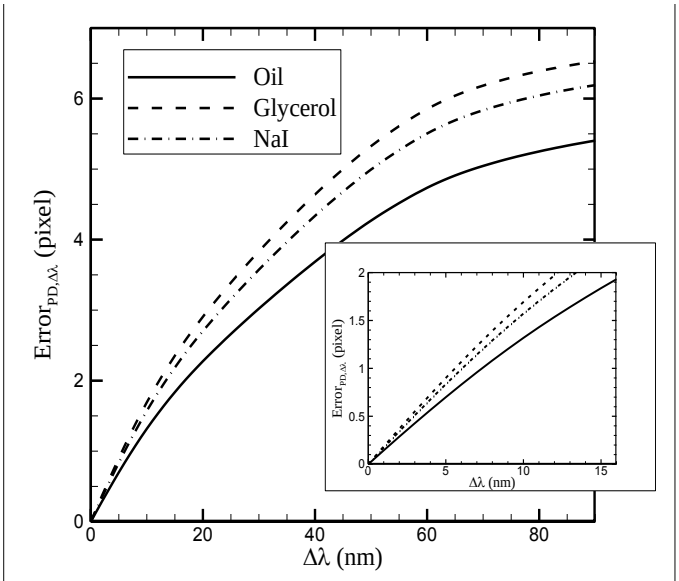

Figure 11. Particle position error versus the detecion light wavelength bandwidth based on Equation (8).

blurred spot merges the multiple images.

CONCLUSIONS

This paper explored some of the position errors and image distortion errors that occur as a function of mismatches of index of refraction when imaging in a porous bed. Trends are shown illustrating the magnitude of errors, measured in pixels, which occur when the liquid phase index of refraction is both greater and less than the solid phase. These results are for a porous bed that has a cross section of 40mm x 40 mm using 6mm diameter beads that were randomly packed. The liquid phase was ammonium thiocynate. Errors of an imaged array of dots are shown to be as high as 1 pixel for index mismatching of 0.0005. Multiple images of single dot were detected for index mismatching of 0.002. Since the index of refraction is wavelength dependent, the effect of broadband illumination position errors on the order of one pixel occur if the illumination bandwidth is greater than 10 nm. Illustrative models are used to show the trends in increasing error with increasing index mismatch.

NOMENCLATURE

A	Area
D_B	Diameter of the Pyrex® bead
$Error$	Error in estimating dot center position (pixel)
I	Spatially integrated intensity for the center dot
I_p	Intensity of the pixel 'p'
L	Length of the bed in camera viewing direction
l_M	Distance of the center of mass along the line through the dot to the centroid of the dot
M	Magnification of the optical system
N_B	Number of beads imaged per 1000 pixel
N_m	Number of rows in the dot array
N_n	Number of columns in the dot array
n	Refractive index of the liquid at laser light wavelength of 527 nm
n_D	Refractive index of the liquid at wavelength of 589.3 nm
P	Power of lens
T	Transmittance of the porous bed for the center, 1mm, dot
X	'x' coordinate of the dot center evaluated using centroid method, $\frac{\sum_p X_p}{\sum_p 1}$
X_p	'x' coordinate of the pixel 'p'

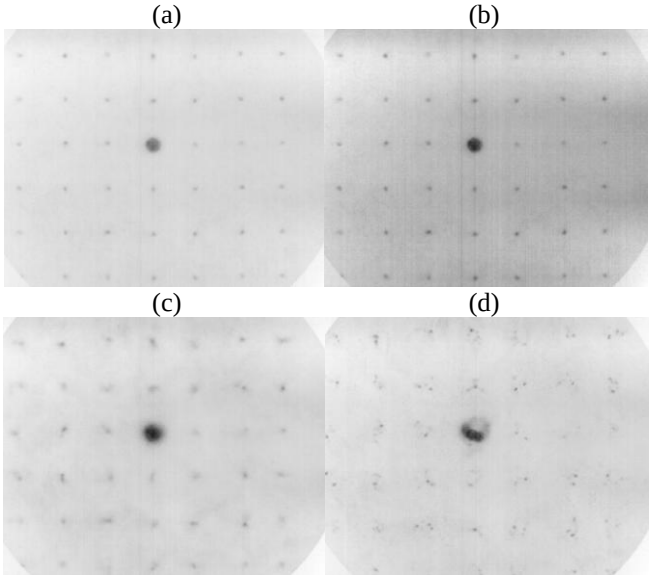

Figure 12. Control experiment used to determine conditions for multiple images; (a) imaged with sodium lamp, (b) same as (a) but with increased contrast, (c) imaged with laser light, (d) same as (c) but refocussed.

Y	'y' coordinate of the dot center evaluated using centroid method, $\frac{\sum_p Y_p}{\sum_p 1}$
Y_p	'y' coordinate of the pixel 'p'
λ	Wavelength of light (nm)
$\Delta\lambda$	Bandwidth of detected light (nm), $\lambda - \lambda_{em}$

Subscript

BED	Porous bed
C-C	Center of the dot matched center of the bead
C-E	Center of the dot matches edge of the bead
CTL	Control image
Dark	Dark image (recorded with no laser light illumination)
e	Element
em	Wavelength of emission maxima
ID	Intensity distortion within a dot
i	Incident light at interface
L	Liquid phase
L-S	Light traveling from liquid to solid at interface
m	row index of dot array
match	Index matched for solid and liquid phases
n	column index of dot array
PD	Position distortion of the dot
refocus	Image where focus was adjusted with beads in the bed
S	Solid phase

S-L	Light traveling from solid to liquid at interface
t	Transmitted light at interface
x	'x' coordinate
y	'y' coordinate
$\Delta\lambda$	Bandwidth of detected light (nm)

REFERENCES

[1] Bear, J., 1988, Dynamics of fluids in porous media, Dover Publications.

[2] Scheidegger, A. E., 1974, The physics of flow through porous media, Universty of Toranto Press

[3] Arthur, J. K., Ruth, D. W., and Tachie, M. F., 2009, "PIV measurements of flow through a model porous medium with varying boundary conditions," Journal of Fluid Mechanics, 629, pp. 343-374.

[4] Northrup, M. A., Kulp, T. J., Angel, S. M., and Pinder, G. F., 1993, "Direct measurement of interstitial velocity-field variations in a porous-medium using fluorescent-particle image velocimetry," Chemical Engineering Science, 48(1), pp. 13-21.

[5] Saleh, S., Thovert, J. F., and Adler, P. M., 1992, "Measurement of 2-dimensional velocity-fields in porous-media by particle image displacement velocimetry," Experiments in Fluids, 12(3), pp. 210-212.

[6] Huang, A. Y. L., Huang, M. Y. F., Capart, H., and Chen, R. H., 2008, "Optical measurements of pore geometry and fluid velocity in a bed of irregularly packed spheres," Experiments in Fluids, 45(2), pp. 309-321.

[7] Lachhab, A., Zhang, Y. K., and Muste, M. V. I., 2008, "Particle Tracking Experiments in Match-Index-Refraction Porous Media," Ground Water, 46(6), pp. 865-872.

[8] Moroni, M., and Cushman, J. H., 2001, "Statistical mechanics with three-dimensional particle tracking velocimetry experiments in the study of anomalous dispersion. II. Experiments," Physics of Fluids, 13(1), pp. 81-91.

[9] Peurrung, L. M., Rashidi, M., and Kulp, T. J., 1995, "Measurement of porous-medium velocity-fields and their volumetric averaging characteristics using particle tracking velocimetry," Chemical Engineering Science, 50(14), pp. 2243-2253.

[10] Stephenson, J. L., and Stewart, W. E., 1986, "Optical measurements of porosity and fluid motion in packed beds," Chemical Engineering Science, 41(8), pp. 2161-2170.

[11] Fontenot, M. M., and Vigil, R. D., 2002, "Pore-scale study of nonaqueous phase liquid dissolution in porous media using laser-induced fluorescence," Journal of Colloid and Interface Science, 247(2), pp. 481-489.

[12] Ovdat, H., and Berkowitz, B., 2006, "Pore-scale study of drainage displacement under combined capillary and gravity effects in index-matched porous media," Water Resources Research, 42(6).

[13] Rashidi, M., Peurrung, L., Tompson, A. F. B., and Kulp, T. J., 1996, "Experimental analysis of pore-scale flow and transport in porous media," Advances in Water Resources, 19(3), pp. 163-180.

[14] Stohr, M., Roth, K., and Jahne, B., 2003, "Measurement of 3D pore-scale flow in index-matched porous media," Experiments in Fluids, 35(2), pp. 159-166.

[15] Johnston, W., Dybbs, A., and Edwards, R., 1975, "Measurement of fluid velocity inside porous-media with a laser anemometer," Physics of Fluids, 18(7), pp. 913-914.

[16] Yarlagadda, A. P., and Yoganathan, A. P., 1989, "Experimental studies of model porous-media fluid-dynamics," Experiments in Fluids, 8(1-2), pp. 59-71.

[17] Khalili, A., Basu, A. J., and Pietrzyk, U., 1998, "Flow visualization in porous media via Positron Emission Tomography," Physics of Fluids, 10(4), pp. 1031-1033.

[18] Ogawa, K., Matsuka, T., Hirai, S., and Okazaki, K., 2001, "Three-dimensional velocity measurement of complex interstitial flows through water-saturated porous media by the tagging method in the MRI technique," Measurement Science and Technology, 12(2), pp. 172-180.

[19] Sederman, A. J., Johns, M. L., Alexander, P., and Gladden, L. F., 1998, "Structure-flow correlations in packed beds," Chemical Engineering Science, 53(12), pp. 2117-2128.

[20] Suekane, T., Yokouchi, Y., and Hirai, S., 2003, "Inertial flow structures in a simple-packed bed of spheres," Aiche Journal, 49(1), pp. 10-17.

[21] Martin, J. J., McCabe, W. L., and Monrad, C. C., 1951, "Pressure drop through stacked spheres. Effect of orientation," Chem. Eng. Progress, 47, pp. 91-94.

[22] Mickley, H. S., Smith, K. A., and Korchak, E. I., 1965, "Fluid flow in packed beds," Chemical Engineering Science, 20(3), pp. 237-246.

[23] McWhirter, J. D., Crawford, M. E., and Klein, D. E., 1998, "Magnetohydrodynamic flows in porous media II: Experimental results," Fusion Technology, 34(3), pp. 187-197.

[24] Raffel, M., Willert, C., and Wereley, S., 2007,

Particle image velocimetry: a practical guide, Springer Verlag.
[25] Budwig, R., 1994, "Refractive-index matching methods for liquid flow investigations," Experiments in Fluids, 17(5), pp. 350-355.
[26] Narrow, T. L., Yoda, M., and Abdel-Khalik, S. I., 2000, "A simple model for the refractive index of sodium iodide aqueous solutions," Experiments in Fluids, 28(3), pp. 282-283.
[27] Lowe, M. L., and Kutt, P. H., 1992, "Refraction through cylindrical-tubes," Experiments in Fluids, 13(5), pp. 315-320.
[28] Feng, Y., Goree, J., and Liu, B., 2007, "Accurate particle position measurement from images," Review of Scientific Instruments, 78(5).
[29] Hecht, E., 2002, "Optics, ed," MA: Addison-Wesley Publishing Company.
[30] Rheims, J., Koser, J., and Wriedt, T., 1997, "Refractive-index measurements in the near-IR using an Abbe refractometer," Measurement Science & Technology, 8(6), pp. 601-605.